Original Research

SLAS Technology
1–15


Automation and Screening
DOI: 10.1177/2472630318776594
journals.sagepub.com/home/jla
SAGE

A Novel Microplate 3D Bioprinting Platform for the Engineering of Muscle and Tendon Tissues

Sandra Laternser[1,2], Hansjoerg Keller[3], Olivier Leupin[3], Martin Rausch[4], Ursula Graf-Hausner[1,2], and Markus Rimann[1,2]

Abstract

Two-dimensional (2D) cell cultures do not reflect the in vivo situation, and thus it is important to develop predictive three-dimensional (3D) in vitro models with enhanced reliability and robustness for drug screening applications. Treatments against muscle-related diseases are becoming more prominent due to the growth of the aging population worldwide. In this study, we describe a novel drug screening platform with automated production of 3D musculoskeletal-tendon-like tissues. With 3D bioprinting, alternating layers of photo-polymerized gelatin-methacryloyl-based bioink and cell suspension tissue models were produced in a dumbbell shape onto novel postholder cell culture inserts in 24-well plates. Monocultures of human primary skeletal muscle cells and rat tenocytes were printed around and between the posts. The cells showed high viability in culture and good tissue differentiation, based on marker gene and protein expressions. Different printing patterns of bioink and cells were explored and calcium signaling with Fluo4-loaded cells while electrically stimulated was shown. Finally, controlled co-printing of tenocytes and myoblasts around and between the posts, respectively, was demonstrated followed by co-culture and co-differentiation. This screening platform combining 3D bioprinting with a novel microplate represents a promising tool to address musculoskeletal diseases.

Keywords

muscle tissue engineering, 3D bioprinting, bioink, drug development, 3D cell culture

Introduction

To enhance the efficiency and success rate of preclinical drug discovery and development, it is important to develop novel three-dimensional (3D) tissue culture models that reflect the in vivo situation better than current two-dimensional (2D) monolayer cell culture systems.[1,2] Organ cultures, such as isolated skeletal mouse muscles, and organotypic cultures, such as hippocampal brain slices, have been known for many years as reliable in vitro tissue assays, allowing functional pharmacology studies.[3–5] However, these assays require animal sacrifice, are highly laborious, and have very low throughput; in addition, reproducibility is limited, and the tissues are very short-lived. As a consequence, very few compounds can be tested per day. To overcome these shortcomings, novel cell culture technologies have been developed to generate multicellular 3D tissue models from different precursor cells. These include spheroids, organoids, cells in scaffolds/hydrogels, and, most recently, cells arranged with 3D bioprinting.[6–9] The formation of spheroids and organoids has allowed the establishment of mouse and human 3D tissue equivalents that demonstrate at least some organ functionality and application as in vitro disease models, particularly in tumor biology.[10,11] While cardiac and smooth muscle cells are able to form spheroids, offering good models for drug development and tissue research,[12–14] skeletal muscle or skeletal-muscle-tendon tissues cannot be fabricated in spheroids as they need a more complex structural and mechanical support.[12] Although skeletal muscle cells are able to form microtissues as shown for the

[1]Competence Center TEDD, Institute of Chemistry and Biotechnology (ICBT), Zurich University of Applied Sciences, Waedenswil, Switzerland
[2]Center for Cell Biology & Tissue Engineering, Institute of Chemistry and Biotechnology (ICBT), Zurich University of Applied Sciences, Waedenswil, Switzerland
[3]Musculoskeletal Diseases, Novartis Institutes for BioMedical Research, Basel, Switzerland
[4]Biotherapeutic and Analytical Technologies, Novartis Institutes for BioMedical Research, Basel, Switzerland

Received Dec 22, 2017, and in revised form Apr 9, 2018. Accepted for publication Apr 16, 2018.

Supplemental material is available online with this article.

Corresponding Authors:
Markus Rimann, Institute of Chemistry and Biotechnology (ICBT), Zurich University of Applied Sciences, Campus Reidbach, Einsiedlerstrasse 31, 8820 Waedenswil, Switzerland.
Email: markus.rimann@zhaw.ch

Hansjoerg Keller, Novartis Institutes for BioMedical Research, Fabrikstrasse 16-1.72.02, 4002 Basel, Switzerland
Email: hansjoerg.keller@novartis.com

propagation of mice and human myoblasts in myospheres,[15–17] the actual differentiation was performed in 2D. Besides manual production of skeletal tissues using hydrogels as proposed by Huang et al.,[18] the rapidly advancing 3D bioprinting technology provides a new approach as it allows the specific deposition of cells and biomaterials in 3D space.[8,19–22] Currently, there are three main modalities of 3D bioprinting: droplet-, extrusion-based, or laser-assisted bioprinting.[23,24] A critical aspect in bioprinting is the printable scaffold material to mirror the extracellular matrix (ECM), the so-called bioink, which holds the printed cells in 3D space.[25–27] The bioink needs to combine two main properties: (1) good printability and (2) good cell compatibility. To print with high accuracy, meaning homogeneous and consistent bioink lines with defined width and height, the bioink should be inherently stable after printing and polymerize/solidify within seconds to provide shape fidelity. Even more important, the bioink should provide an ECM scaffold resembling the precursor cells' natural microenvironment, with respect to attachment sites and elasticity, to optimally promote cell growth and tissue differentiation.[28] We have recently developed a gelatine methacryloyl (GelMA)–based bioink that is printable in extrusion mode as well as with the inkjet printing technology. The bioink is cell compatible, sterile, ready to use, and photo-polymerizable.[29,30]

In our aging society, there is a huge medical need for therapies against degenerative muscle and tendon diseases, which are rapidly increasing in incidence. Furthermore, fatal inherited skeletal muscle diseases, such as Duchenne muscular dystrophy, still lack disease-modifying medication.[31] One of the hurdles in discovering and developing drugs against muscle and tendon diseases is the lack of functional in vitro tissue models that are easy to use, are reliable for compound screening, and show high translatability of the results to standard animal models and ultimately to the clinic.[32–34] Currently, assays with the highest in vivo translatability are ex vivo organ bath assays using isolated mouse muscles, rat tendons, and other contractile tissues as the standard pharmacological tool used in industry. These assays allow force and elasticity measurements and were developed more than 100 years ago.[35–38] However, they require animal tissues, the experiments are very low throughput because tissue preparation is laborious, and experiment number per tissue sample is limited. Classical 2D cell cultures and differentiation of muscle cells into myotubes have been known for many years. It has allowed high-throughput screening of compounds modifying basic aspects of muscle cell growth and function. However, 2D muscle cell culture assays do not permit the screening for core muscle tissue functionality such as force and fatigue. It is challenging to reproduce the dynamic nature of muscle tissues in vitro that show muscle-like geometry, excitability, and contractility. The first cylindrical 3D muscle models, called myooids, were created by placing spontaneously self-assembling and differentiating primary rat myogenic precursor cells between two artificial tendons. They showed spontaneous and induced contractility.[39] One drawback of this method is the use of rat cells hindering translation of drug screening results to humans. Furthermore, the laborious preparation of the experimental setup, including the preparation of the culture dish with suture fixation and sterilization thereof, as well as manual cell seeding, is not suitable for medium- or high-throughput drug screening. In addition, the myooid formation success rate is strongly dependent on the laminin coating, which influences the reproducibility of the models.[39] Similar cylindrical 3D muscle models were fabricated with casting of collagen I/Matrigel cell mixtures into silicone rubber molds containing stainless steel pins,[40] fibrin gel substrates with silk suture anchors,[18] or flexible PDMS posts.[41] The elaborate preparation of the culture dishes, sutures, and posts mentioned above hampers their usage in medium- or high-throughput drug screening. The manual handling of the cells and hydrogels not only is limiting the reproducibility of model fabrication but also is time-consuming compared to automated methods like the bioprinting technology. The fibrin gel-induced self-assembly method was also used to produce functional ligament tissue models from chick tendon fibroblasts between brushite anchors.[42] Functionality of fibrin/Matrigel-engineered rodent muscle tissue models was shown in vivo by vascular integration and increasing force generation of implanted tissue.[43] Furthermore, similarly engineered human 3D myofiber tissue models mimicked pharmacological responses of human skeletal muscle in the clinic.[44] The Matrigel- and fibrin-based hydrogel procedures that are used for muscle tissue production discussed above[18,40–44] are very difficult to handle because it involves manual steps. To increase assay robustness, it is important to automate the process in a controlled environment, as in many applications, the hydrogel properties (stiffness, porosity, etc.) and polymerization are temperature dependent,[45,46] which can influence the reproducibility of the results. All of these assays have some shortcomings concerning limited production capacity, reproducibility, reliability (mouse and rat models), and throughput that are addressed with our developed platform in order to be suitable for compound screening.

In this study, we describe the development of a novel microplate 3D bioprinting platform for the automated production of 3D musculoskeletal-tendon-like tissues for compound screening in drug discovery and development.

Materials and Methods

Cells and Cell Culture

Primary human skeletal-muscle-derived cells (SkMDCs; SK-1111, 17-year-old donor) and MyoTonic Basal medium with growth supplements (MK-2288) for proliferation were purchased from COOK MyoSite (Pittsburgh, PA). The basal medium was supplemented with 20% fetal bovine serum

(FBS) (batch no. 1233705; Gibco, Langley, OK, USA), 10 µg/mL insulin (Art. No. 5-79F00-G; Amimed, Allschwil, Switzerland), and 50 µg/mL gentamicin (Art. No. 15750-037; Gibco). Cells were differentiated using Dulbecco's modified Eagle's medium (DMEM) high glucose with pyruvate (Art. No. 31966-021; Invitrogen, Manchester, UK) containing 2% heat-inactivated horse serum (Art. No. 26050-070; Invitrogen), 1% FBS (batch no. 1233705; Gibco), 1% chicken embryo extract (Art. No. 2850145; MP Biomedicals, Santa Ana, CA, USA), and 50 µg/mL gentamicin (Art. No. 15750-037; Gibco). Cell incubator conditions were 37 °C and 5% CO_2 for proliferation and 37 °C and 7.5% CO_2 for differentiation.

Primary rat tail tenocytes were enzymatically (collagenase IV digestion) isolated from the tail tendon of 17-week-old male rats. They were grown in DMEM high-glucose medium (Art. No. 41965-039; Gibco) containing 20% heat-inactivated FBS, 1% penicillin/streptomycin (Art. No. 15140-122; Gibco), 1% nonessential amino acid (Art. No. 1114; Gibco), and 0.1% β-mercapto-ethanol (Art. No. 31350-010; Gibco). Tenocyte monoculture differentiation was induced with DMEM/F12 Glutamax (Art. No. 31966-021; Invitrogen) containing 1% N2-Supplement (17502-048; Invitrogen), 0.75% L-Ascorbic Acid Phosphate Magnesium Salt n-Hydrate (Art. No. WA3013-19641; Wako, USA) and 1% penicillin/streptomycin. Culture conditions for proliferation and differentiation were 37 °C and 5% CO_2.

Insert Development and Fabrication

The 24-well plates were designed and produced by Weidmann Medical Technology AG (Rapperswil, Switzerland) made of untreated polystyrene (PS) according to the standard footprint of the Society for Laboratory Automation and Screening (SLAS). Weidmann also developed the postholder inserts by injection molding made of polypropylene (PP) with two round-shaped posts for tissue attachment (**Fig. 1D**,**E**). The post distance was 8.3 mm. The thickness of the round posts was at both ends 0.75 mm and in the middle 0.5 mm, with a height of 5 mm (**Fig. 1C**).

The inserts were fixed by two guidelines in the wells (**Fig. 1A**,**B,E**) and were embedded into a 0.8% agarose (A9918; Sigma-Aldrich Chemie GmbH Buchs, Switzerland) gel solution to print on an even and flat surface between the two posts while maintaining optical transparency (**Fig. 1F,G**). The agarose powder was dissolved in serum-free MyoTonic Basal medium. To enable the production of a flat agarose surface around the postholder, different plasma treatment patterns were investigated to selectively enhance hydrophilicity of the material. Embedding tests with (1) plasma-treated plates and treated inserts, (2) untreated plates and treated inserts, and (3) plasma-treated plates and untreated inserts were performed compared to (4) both untreated plates and inserts. SuSoS AG (Dübendorf, Switzerland) did the plasma treatment. The best condition for a flat and even agarose surface was untreated plates with treated inserts.

Bioprinting System

Development of a cell-stirring system. To print homogeneous cell concentrations for >1 h, a cell-mixing system was developed together with regenHU Ltd. (Switzerland) to avoid cell sedimentation in the printing cartridge. This stirring system, developed in the project frame, is now commercially available at regenHU Ltd. The stirrer was 3D printed using PA2200 material, a commonly used polyamide, with five propeller triplets (**Fig. 2C**,**D**) connected to the motor control unit. PA2200 is cell compatible and ethanol resistant, which is important for sterilization and reuse. The modular stirring system fits into a 3-mL printing cartridge (3-cc cartridge; regenHU Ltd). Stirring speed is continuously adjustable between 0 and 240 rpm. To analyze stirring effect on cell concentration and viability, cells were printed/jetted through the jetting valve, harvested at different time points, and analyzed for viability and cell concentration with the cell counting device CEDEX (Roche, Innovatis, Basel, Switzerland). Samples of printed/jetted cells through the jetting valve but without stirring system served as a control.

3D printing of muscle and tendon monoculture tissues. Cells and bioink were printed using the 3DDiscovery (regenHU Ltd.). Two different bioink compositions were synthesized at ZHAW according to a published protocol.[25] The first bioink was a gelatine methacryloyl-polyethylenglycol dimethacrylate (GelMA-PEGDMA)-based ink, termed GP5, with 5% GelMA and 5% PEGDMA (cat. No. 15178; Polysciences, Hirschberg an der Bergstrasse, Germany) in PBS (methacryloyl degree 90%). The second bioink was pure GelMA based, termed G5, with 5% GelMA in PBS (methacryloyl degree 90%). The bioinks were printed in contact mode, about 0.1 mm above the surface, using a reusable extended needle (inner diameter 0.3 mm, length 22 mm) (**Fig. 2B**) with a resolution of about 0.3 mm. A cartridge temperature control system (regenHU Ltd.) was used to print bioinks at 20 °C to have constant printing conditions (e.g., viscosity). Both bioinks were photopolymerizable with UV light (365 nm) after printing, using the photoinitiator lithium phenyl-2,4,6-trimethylbenzoylphosphinate (LAP).[47] For polymerization, the UV LED pen integrated in the bioprinter illuminated the structure by moving along the printed structure at a speed of 5 mm/s for about 20 s. Cells were jetted into the wells with a distance of 2 cm through a valve with an orifice diameter of 150 µm. Droplet volume was about 10 nL. A pressure of 750 to 1000 hPa for bioink printing and 250 hPa for cell jetting was applied.

Tenocytes or myoblasts in monolayer culture were detached with trypsin, suspended in basal media containing

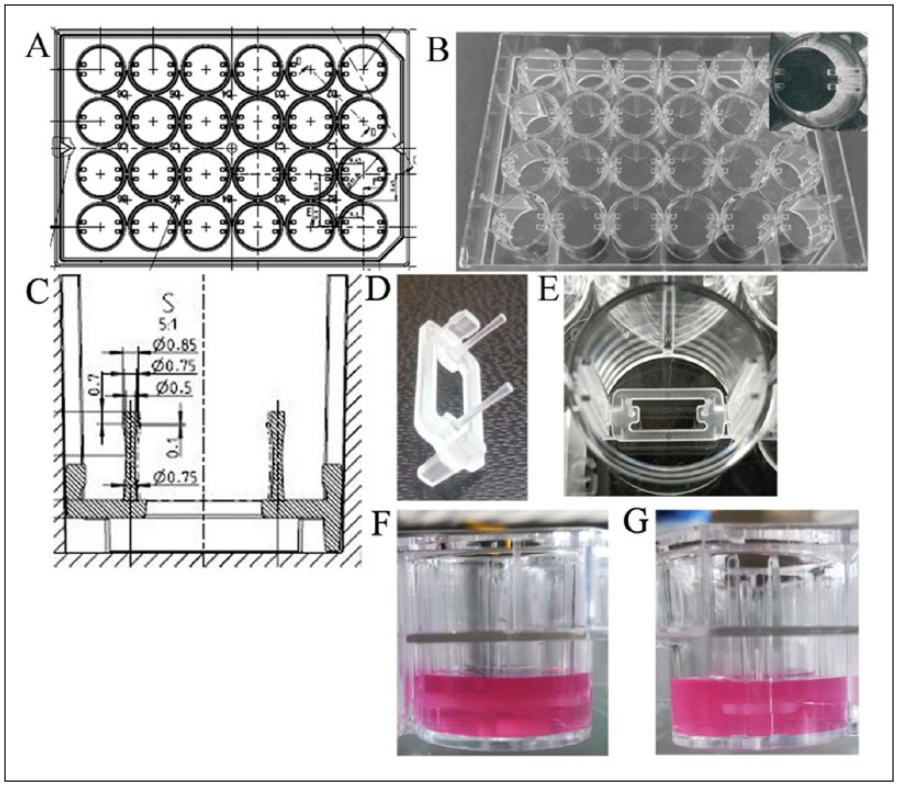

Figure 1. Novel multiwell plate device designed for three-dimensional muscle-tendon tissue printing. (**A**) Schematic drawing of a 24-well plate with guidelines on both sides of each well for postholder insert fixation. (**B**) Injection-molded 24-well plate made of polystyrene (PS), bottom view. Inset: closeup view of one well with guidelines. (**C**) Drawing of fenestrated postholder insert with round-shaped posts, inserted into a well of a 24-well plate, side view of one well. The numbers are the dimensions in mm. (**D**) Injection-molded postholder insert made of polypropylene (PP). (**E**) Postholder insert fixed in the well with the guidelines. Postholder inserts embedded into 0.8% agarose containing phenol red, (**F**) front view, (**G**) side view.

supplements to obtain 2×10^7 cells/mL, and subsequently filled into printing cartridges, where afterwards the stirring unit was inserted. Cells and bioinks were printed in dumbbell lines according to computer-aided design (CAD) drawings generated with the integrated BioCAD program (regenHU Ltd.) as shown in **Figure 2A**,**G,H** on the agarose surface around the embedded posts. The dumbbell-shaped structure was about 1 cm in length (**Fig. 2A**). One layer of bioink was deposited and photo-polymerized on the agarose surface followed by a layer of jetted cell suspension. This process was alternated to result in a total of five bioink layers and four cell layers, which was defined as a standard dumbbell-shaped structure/model. Printed models were cultivated the first 2 days in proliferation and afterwards in differentiation medium. Depending on the experiment, the models were analyzed at differentiation days 4, 7, 14, and 22.

Various printing patterns were designed and analyzed concerning fiber alignment, functionality, and differentiation as described below. Besides the standard dumbbell-shaped structure comprising five layers of bioink and four cell layers, as described above, a two-layer dumbbell-shaped structure, a cross-strip structure, a container structure, a two-channel structure, and a bioink-free structure (only cell suspension around the posts) were printed. The cross-strip structure was printed by splitting the middle part into five strips. The gap between the strips was about 0.5 mm. This was measured after printing by image analysis, to confirm structure fidelity and printing resolution (bioink line thickness and shape). For the container structure, a dumbbell-shaped container was printed by printing a bottom layer, followed by seven borderline layers on top of each other to produce a wall. The container cavity was about 1 mm wide and filled with a jetted cell suspension and subsequently closed by printing a top layer of bioink. The two-channel structure was printed in the same way but with a middle rim dividing the 1-mm-wide container into two tubular structures of about 0.3 mm in width. This was measured after printing by image analysis, to confirm structure fidelity and printing resolution (bioink line thickness and shape). The bioink-free muscle model was printed by jetting five "layers" of cell suspension around the posts in the standard dumbbell shape.

Co-culture printing to generate muscle-tendon tissues. To print co-cultures of myoblasts and tenocytes, both cell types were filled into two separate cartridges and were printed in separate areas on bioink layers (GP5 and G5) building the standard dumbbell-shaped structure, with five bioink layers and four cell layers. Tenocytes were printed around the posts, whereas the myoblasts were printed between the posts, in the middle part of the structure. Myoblasts and tenocytes were printed with a gap of about 0.3 mm. The gap was introduced to get a clear border between the two cell types. To investigate printing accuracy, cells were prestained with

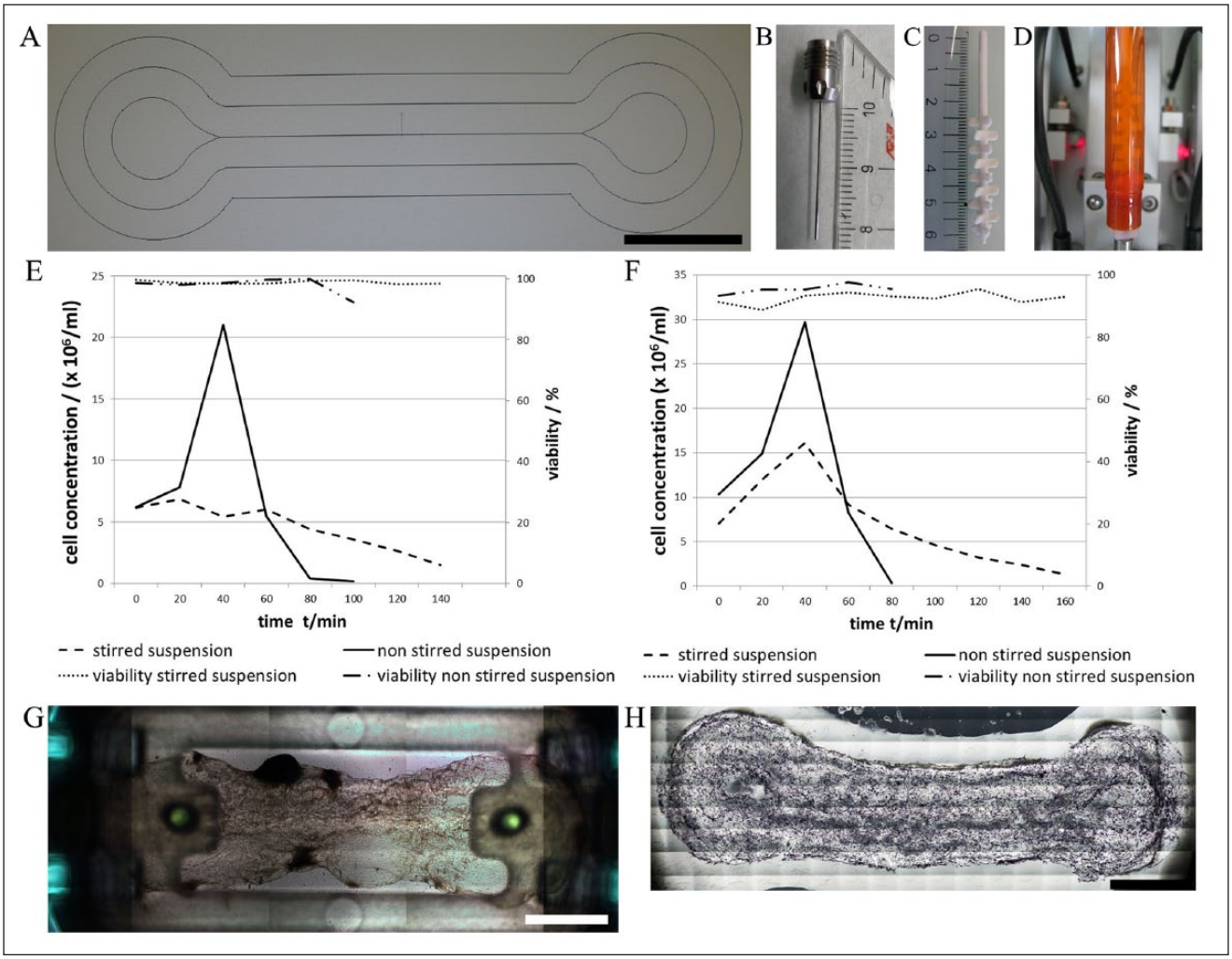

Figure 2. Three-dimensional bioprinting of myoblasts and tenocytes. (**A**) Computer-aided design (CAD) structure of one layer of bioink printed in contact mode with a long needle shown in (**B**). The measures are in cm. (**C**) Cell suspension stirrer. The measures are in cm. (**D**) Stirrer inserted into a printing cartridge with cell suspension. (**E**) Concentration and viability of printed myoblasts with and without stirring system over 140 min. Stirring speed: 240 rpm. (**F**) Concentration and viability of printed tenocytes with and without stirring system over 160 min. Stirring speed: 240 rpm. (**G**) Bright-field image of a printed myoblast model with G5 on a postholder insert embedded into 0.8% agarose solution after 7 days of differentiation. (**H**) MTT (Methylthiazolyldiphenyl-tetrazolium bromide, 1 µg/mL in phosphate buffered saline solution (PBS)) viability staining of a myoblast model with GP5 after 7 days in proliferation. Scale bars (**A**, **G**, and **H**): 2 mm.

CellTracker green and red (Art. No. C7025 and C34552, respectively; Invitrogen), and their positions were analyzed after printing by fluorescence microscopy imaging with an Olympus (Volketswil, Switzerland) IX81 microscope. Printed myoblast/tenocyte co-cultures were grown and differentiated using the muscle differentiation media. Depending on the experiment, the models were differentiated for up to 7 days before analysis.

Immunohistology. Tissue models were fixed with 10% formalin (HT501128; Sigma) for 45 min. Cell nuclei were stained with propidium iodide (Sigma). For immunostainings, models were first blocked in 10% normal goat serum (Art No. 14190; Invitrogen) for 30 min. Primary antibody incubation was then performed for 1 h using antibodies against myosin heavy chain (MHC, clone A4.1025, Art No. 05-716; Millipore, Darmstadt, Germany) and α-actinin (monoclonal anti–α-actinin antibody, Art No. A7811; Sigma), both with a dilution of 1:500 in 0.1% Triton X-100/PBS. After washing with PBS, models were incubated with secondary antibody Alexa Fluor 488 (F(ab')2 Fragments, Art No. A11017; Invitrogen) diluted 1:500 in 0.1% Triton X-100 in PBS for 1 h. F-actin staining (BODIPY FL phallacidin, Art No. B-607; Invitrogen) was done after the blocking step (1% bovine serum albumin [BSA], 0.1% Triton X-100 in PBS) for 20 min. BODIPY was diluted in blocking buffer (1:40) and was incubated for 20 min. Collagen I and III immunostainings were performed after a

45-min blocking step of 1% fetal bovine serum (FBS) and 0.1% Triton X-100 in PBS. Primary antibodies against collagen I and III (Art No. 600-401-103 and 600-401-105, respectively; Rockland, Limerick, PA, USA) were incubated overnight at 4 °C (diluted in blocking buffer 1:500). After PBS wash, secondary antibody Alexa Fluor 488 (diluted in blocking buffer 1:500) was incubated for 1 h. Images were recorded using the fluorescent microscope Olympus IX81, with the software CellSense Dimensions V1.13 and the confocal laser scanning microscope Olympus IX81 FLUOVIEW FV 1000, with the software FLUOVIEW Ver.4.2a. To verify tissue model differentiation and staining specificity, proliferation models as well as negative controls (without primary antibody) were analyzed.

Electrical pulse stimulation and Ca^{2+} imaging of muscle models. Two-channel muscle models were loaded with 5 µM Fluo-4 AM and 0.04% Pluronic F-127 (both from ThermoFisher, Canoga Park, CA, USA) in differentiation medium for 30 min at 37 °C. Subsequently, tissue models were electrically stimulated using U-shaped platinum electrodes that were placed to the muscle strand in parallel. Bipolar electrical pulse stimuli were used to activate muscle contraction. The parameters of these stimuli were as follows: 1-ms pulse length, 50-Hz stimulation frequency, 300-ms pulse train length, and 16-V stimulation amplitude. Imaging was carried out on a Zeiss (San Diego, CA, USA) Axiovert 200M using a Zeiss A-Plan 5× NA 0.12 lens. Movies were recorded using a Zeiss AxioCam MRm.

Electrical stimulation on standard dumbbell-shaped muscle models (mono- and co-cultures) were made by placing one tinned cooper electrode on each side of the muscle model. The linear electrodes were placed to the muscle strand in parallel. The electrodes were inserted into the media through two holes in the lid. Electrical stimuli were applied with a 4- to 70-Hz stimulation frequency and with a 0.1- to 30-V stimulation amplitude. Movies were recorded using an Olympus IX 81 microscope, with a DP72 camera and the software Olympus Cellsense Dimensions V1.13.

Quantitative PCR gene expression analysis. Total RNA from muscle tissue models was extracted using FastPrep FP120 (Qbiogene, USA) homogenization for frozen samples in combination with the RNeasy kit (Qiagen, Hilden, Germany). Total RNA from tendon models was extracted using Freezer/Mill 6870 (SPEXSamplePrep; Metuchen, NJ, USA) and TRIZOL (ThermoFisher) extraction. RNA expressions were determined by quantitative PCR (qPCR) using the High Capacity cDNA kit (Lithuana), Universal PCR Master mix, and corresponding TaqMan Assays, all from Applied Biosystems (USA). Muscle gene expressions were normalized using the geomean of 18S RNA, GAPDH, TBP, and β2M housekeeping gene expressions. Tenomodulin expression was normalized using Eif4a2 housekeeping gene expression. Three tissue models were analyzed per time point, with the exception of day 4 muscle proliferation models ($n = 2$). Mean and standard error of mean (SEM) were calculated. qPCR analysis has been repeated three times for muscle and tendon tissue models in independent experiments to verify reproducibility of differentiation and tissue engineering.

Results

Microplate and Postholder Insert Development

Our intention was the development of a standard cell culture multiwell plate with novel postholder inserts for the anchoring of in vitro 3D bioprinted muscle/tendon tissue models in the size of a small mouse muscle such as the extensor digitorum longus (EDL) muscle. This allows at least low-throughput functional compound screening. EDL muscles are about 10 mm in length, are 1 to 2 mm in diameter, and can produce maximal forces on the order of 300 to 400 mN.[4] Thus, we have conceived a 24-well plate with standard SLAS footprint that contains lateral guiding rails in each well for the insertion of cell culture inserts with two vertical posts at an 8.3-mm distance (**Fig. 1A–E**). Plates and inserts were devised by computer-aided design and were produced by injection molding using PS and soft PP, respectively. To allow imaging of the tissues between the posts by inverted microscopy, inserts possess a large opening of the mounting plate between the posts (**Fig. 1D**,**E**). To print cells and bioink on these fenestrated inserts at a defined height, the inserts were embedded in optically translucent 0.8% agarose gels up to half height of the posts. In addition, the posts with a total height of 5 mm are concave with a middle diameter of 0.5 mm in comparison to 0.75 mm at the base and top. The concave form should hold the printed tissue models at half height of the posts, thus avoiding the liftoff during cultivation. To reduce hydrophobicity, both inserts and plates were plasma treated. However, this led to an inacceptable concave ("smiling") agarose surface in the whole well (data not shown). In contrast, the use of plasma-treated inserts in nontreated plates resulted in even print-suitable agarose surfaces (**Fig. 1F**,**G**). In summary, a novel 24-well plate with postholder inserts was developed that allows the 3D bioprinting of muscle/tendon models between the posts at half height on an agarose bed and enables imaging of the developing tissues by inverted microscopy.

3D Bioprinting of Muscle and Tendon Monoculture Tissue Models

Muscle and tendon tissue models were 3D bioprinted in alternating layers of photo-polymerized bioink and cells similarly as recently described for full-thickness skin models.[30] To fit the tissues around the two posts of the insert, the

print form was a dumbbell shape (**Fig. 2A**). In total, four layers of cells were printed in a z-direction between five layers of bioink per model, as defined as the standard dumbbell-shaped model. Two different bioink compositions were used for printing muscle and tendon models. The two bioink compositions (GP5 and G5) were selected, after initial bioink composition tests with seven different composed bioinks, in which GelMA concentration and PEGDMA content were varied (data not shown). GP5 and G5 showed the best results for both cell types, tenocytes and myoblasts, concerning biocompatibility (viability staining, MTT (Methylthiazolyldiphenyl-tetrazolium bromide, 1 µg/mL in phosphate buffered saline solution (PBS)), cell spreading in the bioink, and proliferation over 6 days of cultivation. Both bioinks were printed in contact mode using a long needle (**Fig. 2B**), and cells were printed by inkjet mode in droplets of about 10 nL. Printing required about 5 min for one model and about >2 h for a full 24-well plate, respectively. The printed primary skeletal myoblasts (SkMDCs) and tenocytes showed >95% viability (**Fig. 2E**,**F**). However, the concentration of the printed cells rapidly rose from the initial test concentrations of SkMDCs (5×10^6 cells/mL) and tenocytes (10×10^6 cells/mL) that were loaded into the cell cartridges, reaching a peak of 20 to 30×10^6 cells/mL after a 40-min printing time. After 80 min, a fast decline of printed cell concentration down to zero was observed. An explanation for this behavior could be cell sedimentation in the cartridge with ultimate blocking of the printing valve. Thus, we developed together with regenHU Ltd. a cell-stirring system for the cell cartridges (**Fig. 2C**,**D**), which is now commercially available through regenHU Ltd.. The system consists of a stirrer with five staggered triplet propellers made of biocompatible PA2200 material that fits into the cell cartridge. The top of the stirrer was mounted into an electrical motor that serves also as a tight cartridge lid. As expected, cell printing tests with the stirring system showed relatively constant printing cell concentrations for up to 2 h (**Fig. 2E**,**F**, dashed lines). The concentrations of the printed cells dropped only by about 50% at 2 h compared to the initial loaded concentrations. **Figure 2G** shows a picture of a 3D bioprinted dumbbell-shaped model of myoblasts with G5 after 7 days of differentiation on a postholder insert. In addition, MTT staining showed viable muscle cells in a standard dumbbell-shaped structure according to the CAD file lines (**Fig. 2H**). Taken together, a 3D bioprinting procedure was developed that allowed the printing of a full 24-well plate with 3D bioink/muscle and bioink/tendon tissue models on postholder inserts.

Differentiation of Muscle and Tendon Monoculture Models

After printing, 3D cell culture models were maintained in proliferation medium for 1 to 2 days to allow cell adaptation to the new environment and to allow cell growth before initiation of tissue differentiation. Tendon tissue monoculture differentiation was induced by switching to differentiation media for tenocytes, whereas muscle tissue monoculture differentiation was induced by changing to differentiation media for myoblasts. Differentiation was first assessed by marker gene expression analysis using qPCR. Fusion of single-cell myoblasts to multicellular myotubes and maturation into myofibers is characterized by a decrease of the transcription factor Myf5 and induction of myotube-specific genes such as transcription factor myogenin and the structural genes myosin heavy chain (MYH) and α-actinin 2 (ACTN2). Differentiation of tenocytes is characterized by induction of tenomodulin gene (Tnmd). **Figure 3** shows a strong decrease of Myf5 and massive induction of myogenin, MYH2, and ACTN2 in muscle models over 2 weeks when cultured in differentiation medium. In contrast, models incubated in proliferation medium showed much less Myf5 reduction and only very low induction of myotube marker genes (**Fig. 3A–D**). Similarly, tendon models showed massive induction of the Tnmd gene only when incubated in differentiation medium (**Fig. 3E**).

To confirm tissue differentiation and to show tissue structure and maturation in the bioprinted models, we investigated tissue composition and architecture by immunohistology. MHC immunostaining showed formation of multinucleated myotubes throughout the whole models at day 7 of differentiation in GP5 models (**Fig. 4A**,**C**). Furthermore, immunostaining for muscle-specific actin-anchoring ACTN2 and staining for fibrous (f-) actin showed aligned, striated myofibers in G5 bioink models (**Fig. 4D**,**E**). In comparison to differentiated tissues, proliferation models showed no myotube formation, confirmed by negative MHC and ACTN2 staining throughout the whole models as depicted in **Figure 4B** for MHC. Negative controls and proliferation models for ACTN2 were similar. Although GP5 and G5 had different compositions, no impact on myofiber formation and alignment was observed. Taken together, myoblast cell behavior was similar in both bioinks. Tenocyte differentiation was analyzed by collagen I and III immunostainings in G5 (**Fig. 4F**) and in GP5 bioink models (**Fig. 4G**,**I**) and compared to undifferentiated proliferation models (**Fig. 4H**,**J**). Detection of collagen I and III expression demonstrated differentiation of tenocytes at day 7, whereas proliferation models showed no collagen I and III staining (**Fig. 4H**,**J**), and negative controls confirmed staining specificity. Furthermore, no significant differences concerning collagen I or III expression were observed between the two bioinks G5 and GP5, as shown in **Figure 4** for collagen I (**Fig. 4F**,**G**). In summary, marker gene expression and histological analysis showed differentiation of muscle and tendon tissue models. In addition, G5 and GP5 gave the same results for muscle models as well as for tendon models concerning cell differentiation. Therefore, results of GP5 bioink models are mainly presented in the following sections.

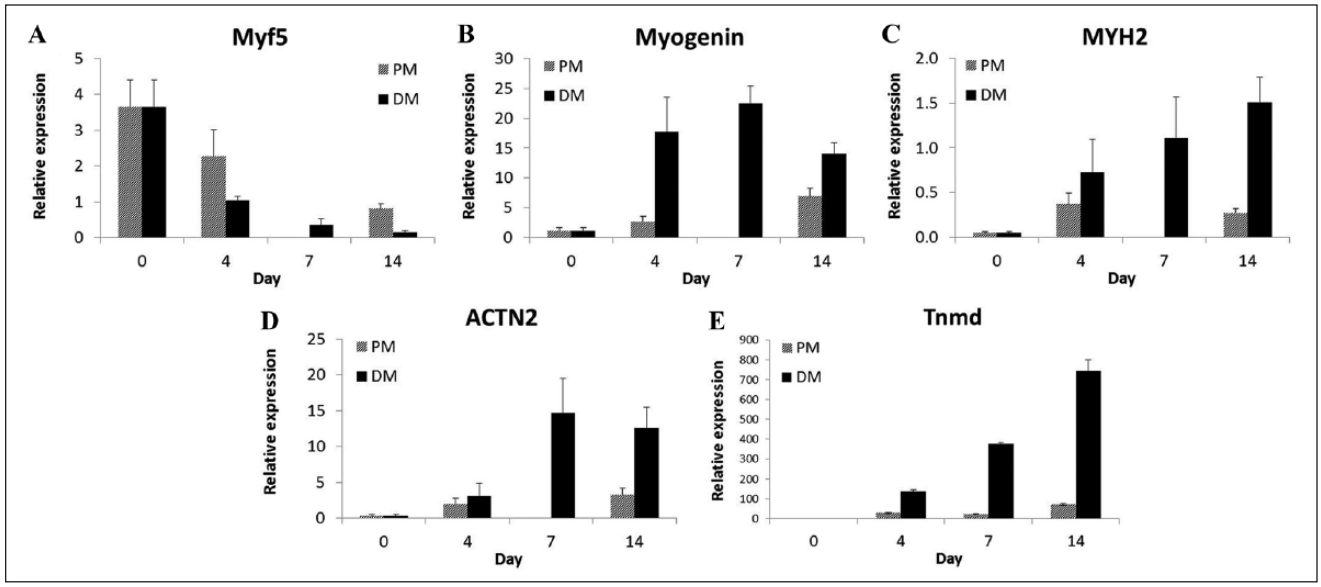

Figure 3. Marker gene analysis of dumbbell-shaped standard muscle and tendon monoculture tissue model differentiation. (**A–D**) Muscle models and (**E**) tendon models were cultured in proliferation medium (PM, gray bars) or differentiation medium (DM, black bars) and were analyzed for corresponding marker gene expressions at different time points as indicated in the figure by quantitative PCR. In graphs **A** to **D**, data points at day 7 of proliferation models are not available. Bars at day 0 in graph **E** have a relative expression of 1 and are not visible in the graph. Three tissue models were analyzed per time point (n = 3), except in day 4 muscle proliferation models (n = 2) in graphs **A** to **D**. Shown are relative expression mean ± standard error of the mean (SEM).

Effect of Print Forms on Muscle Tissue Development and Functionality

To improve the content, density, and alignment of myofibers in the 3D bioprinted tissue models, we explored further print forms beside the standard dumbbell-shaped structure with five layers of GP5 bioink and four layers of cells (**Fig. 5A**) using MHC immunostaining. A minimal two-layer model with two layers of GP5 bioink and one cell layer in between (**Fig. 5B**) showed similar myofiber differentiation as compared to the five-layer model. This indicated that 3D tissue formation was not dependent on the height of the model. Furthermore, a cross-strip model was printed to investigate myofiber alignment. The rationale behind this print form was that myoblasts formed highly aligned myofiber strands bridging bioink gaps of about 0.5 mm in previous experiments. To investigate this behavior, a cross-strip model was printed with bioink strips 0.5 mm apart from each other (**Fig. 5C**). MHC immunostaining of myotubes showed myofiber development at the outside of the model and in the cell layer cross-strips but not or much less in the GP5 bioink cross-strips, indicating that the GP5 bioink is not permissive for muscle cell growth, differentiation, and tissue development. Thus, we tested a container and a two-channel print structure that contained more voluminous cell compartments that were not interrupted by GP5 bioink (**Fig. 5D**,**E**). Both models supported the development of aligned myofibers primarily along the axis of the models between the posts. Fiber alignment and density were best in the two-channel model, as illustrated by a closeup view of myofibers (**Fig. 5F**). The two-channel model with the two bundles of myofibers separated by a rim of GP5 bioink confirmed that GP5 bioink is not permissive for muscle tissue development. Therefore, we explored a print model without any bioink (**Fig. 5G**). Surprisingly, four layers of printed cells remained in place without bioink and even formed muscle fiber–like structures between the two posts after 1 day of cultivation. However, these models became very thin in the middle and tore after 2 to 3 days in differentiation medium.

To show functionality of the engineered myofibers, we analyzed electrically induced Ca^{2+} signaling in two-channel models and electrically induced contraction of standard muscle models. The electrically induced stimulation of standard muscle models differentiated for 6 days showed continuous contraction of single myofibers and groups of myofibers together in the same direction (**Suppl. Video S1**). This confirmed the functionality of the muscle tissue and supported the results of the immunostainings. For the Ca^{2+} imaging, models were loaded with fluorescent Ca^{2+} indicator and stimulated with single rectangular bipolar electrical pulse stimulation (EPS). EPS led to Ca^{2+} signals in the two-myofiber bundles (**Fig. 6** and **Suppl. Video S2**). Fluorescent imaging analysis showed a rapid increase in cytoplasmic Ca^{2+} within milliseconds, followed by a much slower decay of the signal within about 3 s. In summary, print form analysis showed best muscle tissue development between GP5 bioink layers in the two-channel

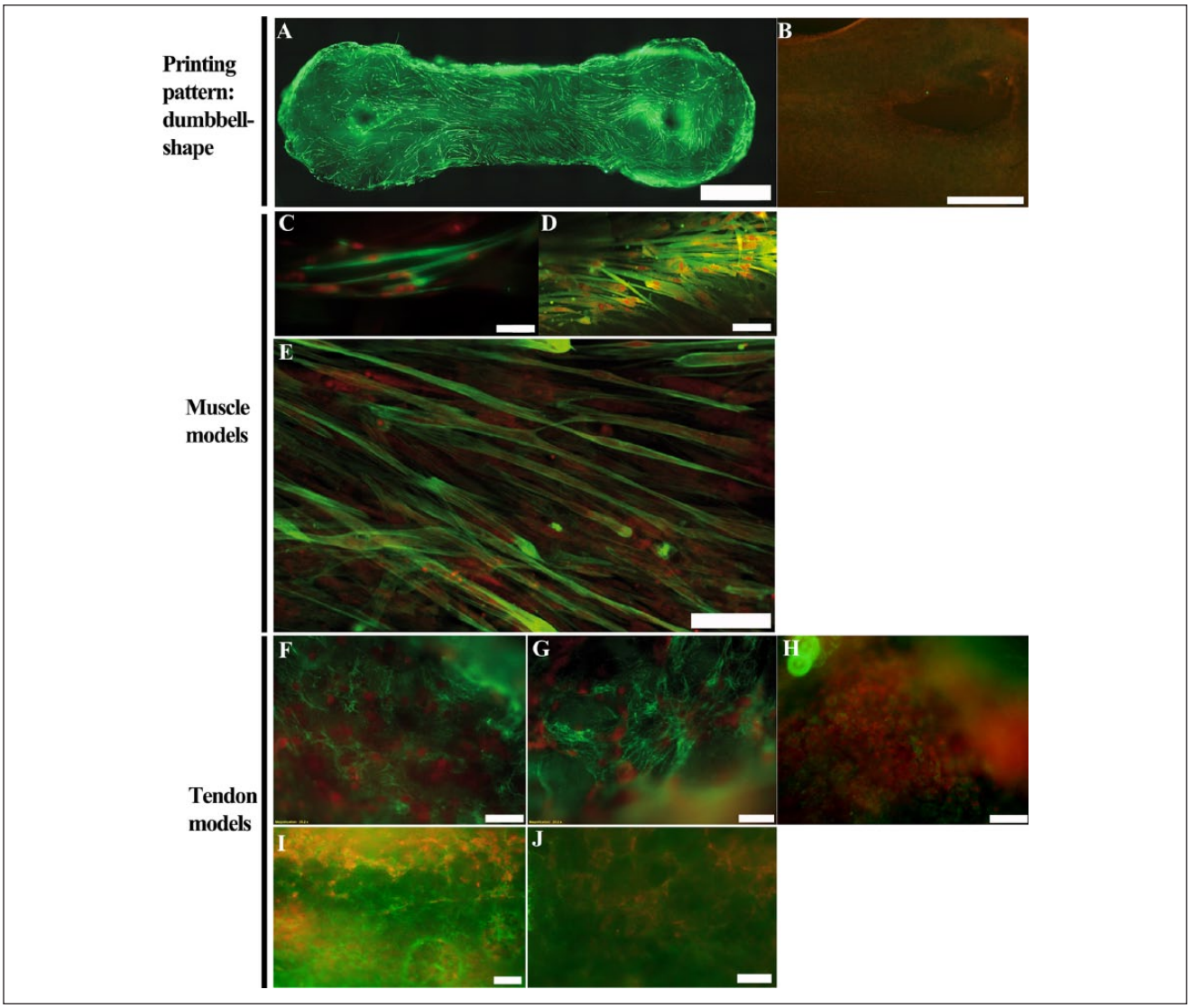

Figure 4. Histological analysis of muscle and tendon monoculture tissue model differentiation. (**A**) A standard dumbbell-shaped muscle model GP5 was differentiated for 7 days (grown for 9 days in total) and was immunostained for myosin heavy chain (MHC). (**B**) Nondifferentiated muscle model stained for MHC after 9 days in culture (proliferation model) (red: cell nuclei stained with propidium iodide). (**C**) Higher magnification of multinucleated and striated myofibers (green: MHC, red: cell nuclei stained with propidium iodide). (**D**) α-Actinin immunostaining (green: α-actinin) and (**E**) f-actin staining (green: f-actin) of a G5 bioink/muscle model differentiated for 14 days (red: cell nuclei stained with propidium iodide). (**F**, **G**) Collagen I staining of tendon models printed with G5 (**F**) and GP5 (**G**) and differentiated for 7 days (grown for 9 days in total). (**H**) For comparison, a proliferation model after 9 days in culture, stained for collagen I (green: collagen I, red: cell nuclei). (**I**, **J**) Collagen III staining of tendon models printed with GP5 (**I**) after differentiation for 7 days (9 days in culture), in comparison to a proliferation model (**J**) after 9 days (green: collagen III, red: cell nuclei). Scale bars: (**A**) 2 mm, (**B**) 1 mm, (**C–G**) 50 µm, and (**H–J**) 100 µm.

model. Functionality of these engineered human myofibers was demonstrated by EPS-induced Ca^{2+} signaling.

3D Bioprinting of Muscle/Tendon Co-cultures

Having generated monocultures of muscle and tendon tissue models, we attempted to generate muscle/tendon tissue co-cultures. Tenocytes were printed around the posts and muscle cells in between to produce organotypic tissue models. To visualize the printed cells and their distribution, tenocytes were prelabeled with CellTracker green and myoblasts were prelabeled with CellTracker red. Fluorescence imaging showed the localization of tenocytes around the posts and muscle cells in between directly after the printing process

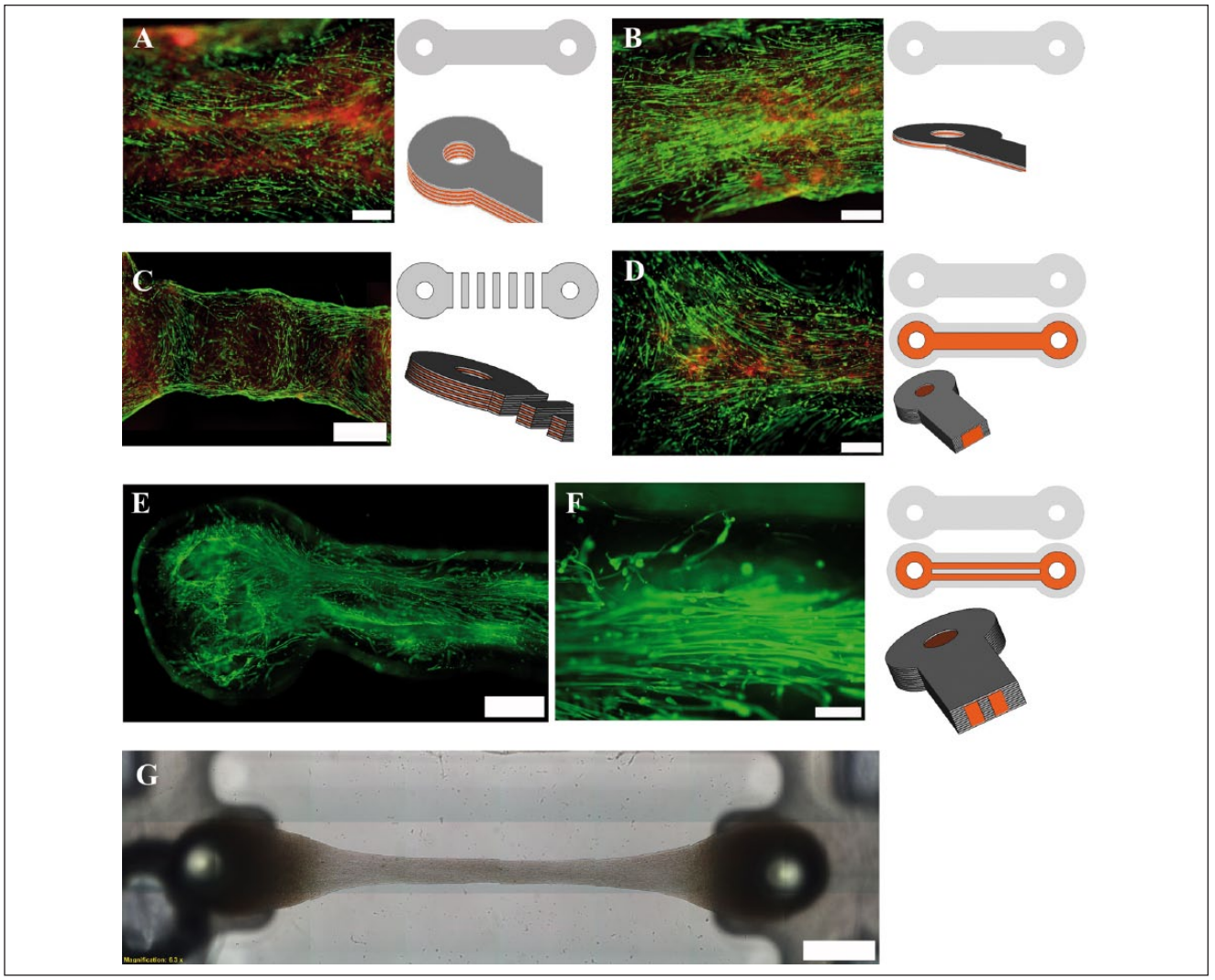

Figure 5. Effect of different print forms on muscle tissue differentiation. Myoblasts were printed using different print forms as shown in the figure and were differentiated for 7 days followed by histological analysis using myosin heavy chain (MHC) immunostaining (green) and propidium iodide nuclear stain (red). (**A**) Standard dumbbell-shaped structure with five layers of GP5 bioink and four layers of cell suspension with schematic top view and side view with different layers (gray: GP5 bioink, orange: cell suspension). (**B**) Two-layer GP5 bioink and one-layer cell suspension with schematic top view and side view. (**C**) Five-strip model with five layers of GP5 bioink and four layers of cell suspension with schematic top view and side view. (**D**) Container structure: GP5 bioink was used as a container (gray) for the cell suspension (orange). Schematic top view and side view. (**E**) Two-channel model: The container model was adapted with a middle line of GP5 bioink as shown in the schematic drawing beside. (**F**) Magnification of one channel of the two-channel model showing bundle-like myofibers aligned in one direction. (**G**) Cell suspension printed without bioink. Muscle cells were jetted on an agarose surface around the posts and cultivated for 1 day. Scale bars: **A**, **B**, and **D**, 500 µm; **F**, 200 µm; and **C**, **E**, and **G**, 1 mm. Video as supplementary file: **Supplementary Video S1**.

with GP5 bioink (**Fig. 7A**). The print lines of the cells were clearly visible. In contrast, the interface between the two cell types was not clearly visible but rather smooth and overlapping, despite the fact that there was a little gap between the two cell types in the CAD print file. To differentiate the tenocytes into a tendon-like tissue part and the myoblasts into the muscle part in the co-culture model, we found the pure muscle cell differentiation medium to be the most suitable. MHC staining of muscle in **Figure 7B** and a collagen I staining of tendon in **Figure 7C** are shown. The co-culture was printed in G5 bioink. In comparison, a negative control for collagen I is shown in **Figure 7C.1**. This verifies the specificity of the collagen I staining. As previously shown, differentiation was assessed for the corresponding monoculture models. In addition, co-culture models differentiated for >7 days showed auto-contractions as well as EPS-induced contractions of single myofibers (**Suppl. Video S3**). To investigate different co-culture model designs, tenocytes were printed with GP5

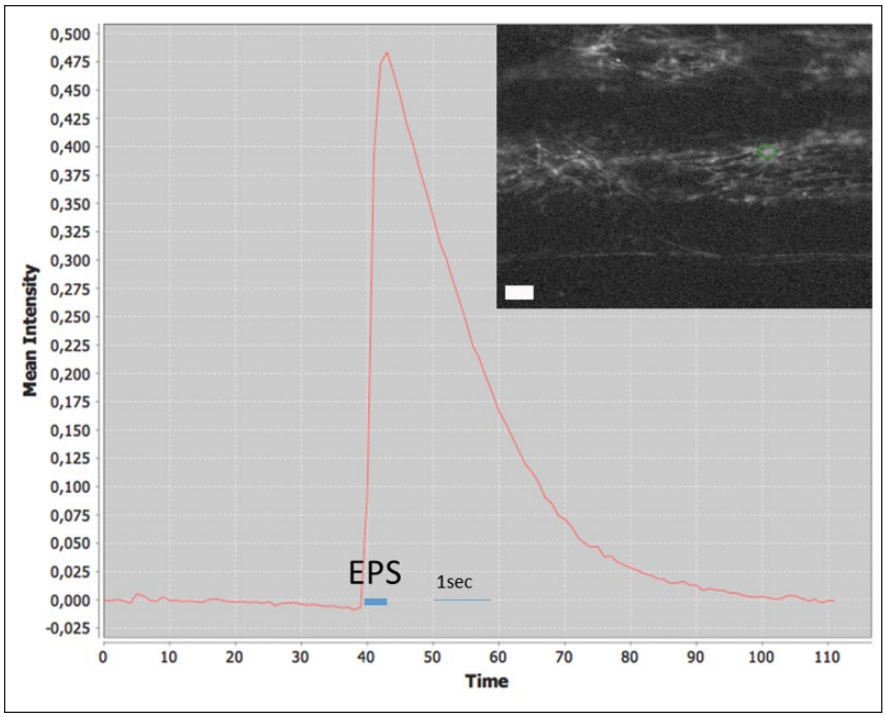

Figure 6. Calcium signaling of printed muscle models. Ca^{2+} imaging of a two-channel muscle model with G5 that was differentiated for 22 days and was loaded with Fluo-4 AM calcium dye. Ca^{2+} signal curve after single electrical pulse stimulation (EPS) of 1 ms duration (300 ms, 50 Hz). Top right: Ca^{2+} signal imaging, while electrically stimulated. The time on the x-axis is in arbitrary units. The length of 1 s is indicated in the figure. The inset demonstrates fluorescent Ca^{2+} signaling in the cytoplasm directly after electrical stimulation. Scale bars: 20 µm. Video as supplementary file: **Supplementary Video S2**.

bioink in a layer-by-layer mode around the posts, and the myoblasts were printed only in cell suspension, without any supporting bioink, between the posts, in the middle part of the structure. After 1 day in proliferation medium, the myoblasts were spanned between the two posts and connected to each other (**Fig. 7D**). In addition, myoblasts formed aligned areas in the muscle part and were able to attach to the tenocyte part. This shows the ability of myoblasts to connect and interact with the tenocyte part. However, the connection tore after 1 to 2 days at one of the GP5 bioink borders. This may show that the myoblast-tenocyte interface was too weak yet to withstand the developed tension in the muscle part, without having produced supporting ECM in the same time.

Discussion

3D bioprinting has a great potential in the engineering of functional 3D tissues in vitro for applications in drug discovery and regenerative medicine. We report herein a novel automated 3D bioprinting system for the generation of skeletal muscle and tendon microtissue models in a standard 24-well plate screening format. To our knowledge, this is the first description of a standardized microwell 3D tissue bioprinting platform for drug screening. The 24-well plate format was chosen to produce muscle tissue models in the same size as mouse EDL muscles, which are commonly used in organ bath assays for in vitro functional compound tests.[4] EDL muscle dissection, preparation, and mounting to force transducers in the superfusion chamber require on average about 1 to 2 h per muscle and allow the testing of only one compound before tissue deterioration. Our 24-well bioprinted tissue platform has the potential to provide medium-throughput screening of compounds for at least some basic functionalities of muscle and tendon tissue, which represent a huge screening increase. In addition, it reduces animal experimentation. Very recently, a related 3D skeletal muscle-on-a-chip platform has been described by Agrawal et al.[48] They used a 3D photo-patterning approach to fabricate skeletal muscle tissue in a cell-laden gelatin network around two hydrogel pillars in a microfluidics chamber. With this in vitro muscle model, they successfully showed functional compound testing. The advantage of our platform in comparison might be the automated fabrication of 24 similar human muscle tissues. This might save time and increase the robustness of drug screening results, due to the production of 24 similar human muscle tissues. Another related platform used engineered muscle tissues around casted flexible PDMS posts in 96-well plates allowing high-throughput functional screening. This platform was originally developed and published by Vandenburgh,[49] who founded the company Myomics, Inc., which is now offering drug screening services together with InvivoSciences LLC[50]. The advantage of our platform in comparison might be the in-house production, screening, and analysis of muscle tissues for drug screening applications without the need to outsource to a contract research organization, which makes the platform more flexible.

The primary human myoblasts and rat tenocytes virtually all survived the printing process as shown by the observed >95% viability after printing. Previously, we have

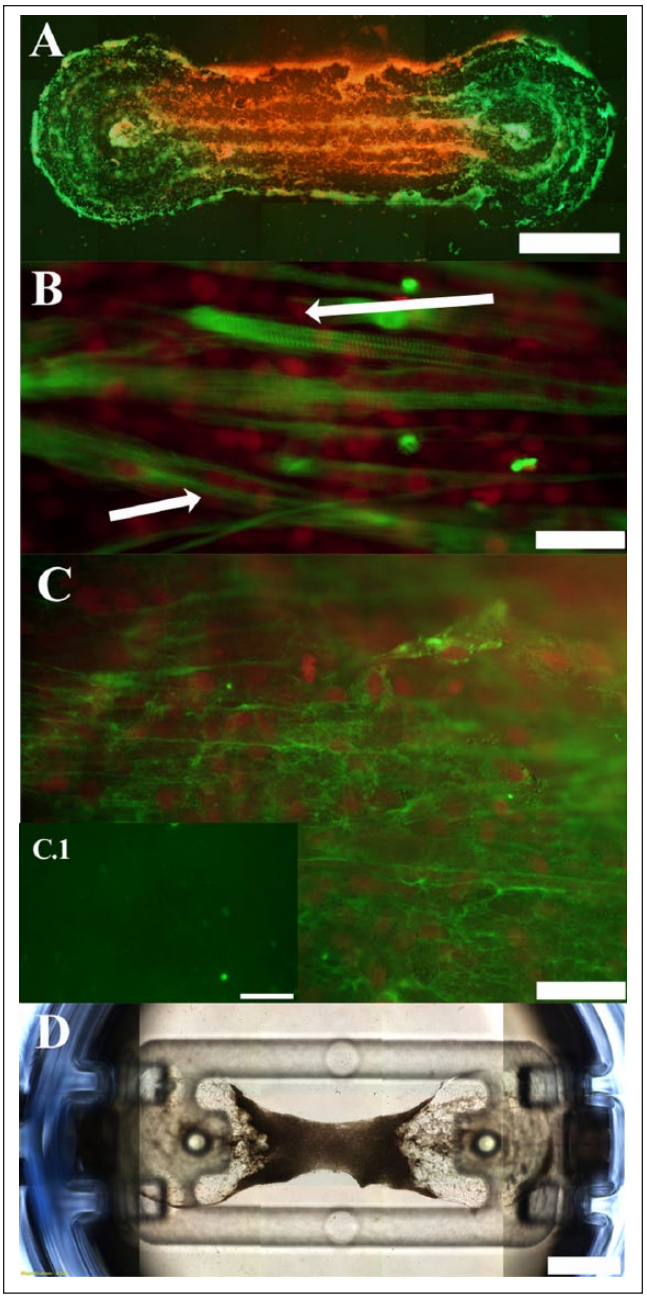

Figure 7. Three-dimensional printed co-culture with tenocytes around the posts and myoblasts in the middle part of the dumbbell-shaped structure. (**A**) Prestained tenocytes (green) and myoblasts (red) directly after printing with GP5 bioink. (**B**) Co-culture model printed with G5 bioink and differentiated for 7 days and stained for myosin heavy chain (MHC) in green (red: cell nuclei). Arrows indicate striated and multinucleated myofibers within the co-culture. (**C**) Collagen I staining in the tenocyte part of the co-culture model printed in G5 bioink and (**C.1**) negative control of collagen I staining in comparison. (**D**) Co-culture overview image (bright field): Tenocytes were printed between GP5 bioink layers around the posts and myoblasts were jetted without any supportive bioink into the middle part between the posts. Scale bars: **A** and **D**, 2 mm; **B** and **C**, 50 µm; and **C.1**, 200 µm. Video as supplementary file: **Supplementary Video S3**.

seen the same survival with primary human dermal fibroblasts using similar printing parameters with a 150-µm valve opening, 250-hPa pressure, and 250-µs valve opening time.[30] However, it is important to verify the optimal printing parameters for any given cell type. Other cell types that show low postprinting viability after inkjet printing might be more susceptible for extrusion printing when cells are printed while mixed in bioink. In this work, the cells were surviving the jetting process without any loss in viability. Printed myoblasts and tenocytes grew in proliferation medium and then differentiated into myotube and tendon-like tissues in the corresponding differentiation media, respectively, as shown by genetic and immunological marker gene expression analysis. Furthermore, the functionality of muscle tissue models was demonstrated by imaging of Ca^{2+} signaling and myofiber contractility. However, histological analysis showed only dispersed thin myofiber development, particularly around the posts. This seems different from in vitro engineered human skeletal muscle models using molding techniques showing many aligned myofibers and whole-model contractions.[44] One of the identified reasons for this is the nonpermissiveness of our bioink for myoblast cell penetration and differentiation, which was shown by our tests with various printing patterns, particularly with the cross-strip model. Therefore, we think that our standard dumbbell-shaped 3D tissue models (five layers of bioink and four layers of cell suspension between the bioink layers) were mainly cell layers stacked in bioink layers. Accordingly, myofiber differentiation was very limited and best in areas that were low or free of bioink. This is also consistent with the observation that the two-channel model with much reduced bioink compartments and larger cell compartments showed best differentiation. These findings clearly demonstrate that developing bioinks that suit every cell type is not possible, since in a previous publication, we demonstrated the cell compatibility of the GP5 with primary human dermal fibroblasts and epidermal keratinocytes.[30] EPS-induced Ca^{2+} signaling in a two-channel model showed the expected, very rapid rise in intracellular Ca^{2+} within about 300 ms, followed by a much slower decay during 4 to 5 s back to baseline. This slow decline of the fluorescence signal and therefore a slow decay of intracellular Ca^{2+} indicated that most myofibers were immature and rather myotube-like in the two-channel model, with nonaligned sarcomeres and little organized sarcoplasmic reticulum and excitation-contraction coupling. Adult and mature muscle fibers usually show a similar strong decline of the fluorescence signal and a respective decay of intracellular Ca^{2+} as the signal increases, whereas younger, myotube-like fibers show a significant slower decline/decay compared to the increase/release of Ca^{2+}. This could be shown in isolated mouse muscle fibers of mice at different ages as well as in isolated human muscle fibers in different development states.[51,52] The slow Ca^{2+}

decay could be due to the lower amount of Ca^{2+}-handling proteins (RyR1 and sarcoplasmic reticulum) present in myotube-like fibers compared to mature human muscle fibers.[52]

Using fluorescent, nontoxic, living cell markers, we have demonstrated the specific, spatial localization of tenocytes around the posts and myoblasts between the posts on the cell culture insert in 24-well plates according to the CAD file design. This nicely illustrates the capability of our 3D bioprinting platform to specifically position different cell types with the help of bioink at any position as defined in the CAD file in the well. Currently, the bioprinter features four printheads allowing printing three different cell types in addition to bioink. The distribution and positioning of the two cell types are better defined and equate more the initial CAD drawing of cell distribution in the middle part and the circle part around the posts than at the cell type interface area, where the two cell types are deposited adjacent to each other. This was analyzed by visual observation directly after the printing process. This may be due to smearing of cells by the bioink layers, which were printed in contact mode. As expected, growth and differentiation of muscle/tendon co-cultures were not trivial in terms of finding a suitable culture media. A 1:1 mixture of myoblast and tenocyte differentiation media resulted in a complete overgrowth of the muscle cells by the tenocytes. Fortunately, pure myoblast differentiation medium allowed myoblast as well as tenocyte differentiation in the co-cultures. Although the two cell types were spatially separated after printing, the cells physically connected at their interface and formed one continuous tissue model. Thus, the interaction and joining of muscle and tendon cells seemed to be a conserved evolutionary process at least among mammals. Although co-cultures of cells from different species have certain advantages, for example, for cell type–specific genetic analysis of cellular differentiation, it will be interesting to investigate pure human co-cultures using human tenocytes as physiologically more relevant models. We believe that our 3D bioprinted muscle-tendon tissue model is a new promising in vitro system to study the structure and function of myotendinous junction formation, development, and homeostasis. Our differentiated muscle models showed spontaneously and EPS-induced contracting myofibers. Although our system is able to generate functional muscle tissue models, the extent, quality, and maturity of the engineered tissue are not yet sufficient for reasonable compound screening. A crucial step in tissue engineering will be the identification and/or development of new hydrogel bioinks that promote 3D muscle tissue formation. Another area of improvement appears to be the postholder cell culture inserts. Although postholder production is feasible in large quantities and at low costs by injection molding, the posts made of PP inserts are too stiff to be bent by the contracting muscle models. This is a prerequisite for an optical force readout for functional compound screening. Thus, softer plastics materials have to be evaluated in the direction of the very soft PDMS posts used by other platforms.[49] Despite these limitations, we think that our new microwell 3D bioprinting platform has great potential as a new microphysiological system to allow automated in vitro drug screening of muscle function regulating compounds.

In conclusion, in this project, we were printing human primary muscle and rat tendon cells within bioink layers to produce 3D muscle and tendon tissue models on postholder inserts in a specialized 24-well plate. Muscle and tendon monocultures were fabricated, showing good differentiation, and the feasibility of printing co-cultures of muscle/tendon tissues was demonstrated. In the co-culture condition, the tendon tissue was developed around the two posts, whereas the muscle tissue was differentiated between the posts adjacent to the tendon tissue. The specialized 24-well plate allowed the production of 24 tissues in about 2 h. The printed muscle tissue was contracting after electrical stimulation, demonstrating biological functionality. We could show that the 3D bioprinting technology opens the doors to produce defined and small functional 3D tissue structures directly in a specialized well plate device. In the future, the specialized 24-well plate will be equipped with electrodes for electrical stimulation to monitor differences in muscle contraction after drug exposure. The development of platforms to produce, maintain/grow, and analyze in vitro 3D tissue models is a first step toward implementation in the pharma industry for drug development applications to increase the throughput and reliability.

Acknowledgments

We thank our collaboration partners Marc Thurner and Andreas Scheidegger (regenHU Ltd.), Kurt Eggmann, Daniel Quidiello, and Thomas Faessler (Weidmann Medical Technology AG) for the contribution of printing technology and labware production expertise. Furthermore, we thank Angela Alaves Reyes-Furrer, Lilian Hartmann, Heidi Jeker, and Jens Richter for muscle and tendon technical expertise.

Declaration of Conflicting Interests

The authors declared the following potential conflicts of interest with respect to the research, authorship, and/or publication of this article: Hansjoerg Keller, Olivier Leupin, and Martin Rausch were employed by the Novartis Institutes for BioMedical Research and their research and authorship of this article was completed within the scope of this employment.

Funding

The authors disclosed receipt of the following financial support for the research, authorship, and/or publication of this article: We thank the innovation promotion agency (CTI, Switzerland Project No.: 16313.1) for financial support and technical guidance.

References

1. Page, H.; Flood, P.; Reynaud, E. G.; et al. Three-Dimensional Tissue Cultures: Current Trends and Beyond. *Cell Tissue Res*. **2013**, *352*, 123–131.
2. Fang, Y.; Eglen, R. M.; et al. Three-Dimensional Cell Cultures in Drug Discovery and Development. *SLAS Discov*. **2017**, *22*, 456–472.
3. Matar, W.; Nosek, T. M.; Wong, D.; et al. Pinacidil Suppresses Contractility and Preserves Energy but Glibenclamide Has No Effect During Muscle Fatigue. *Am. J. Physiol. Cell Physiol*. **2000**, *278*, C404–C416.
4. Moorwood, C.; Liu, M.; Tian, Z.; et al. Isometric and Eccentric Force Generation Assessment of Skeletal Muscles Isolated from Murine Models of Muscular Dystrophies. *J. Vis. Exp*. **2013**, *71*, e50036.
5. Li, Q.; Han, X.; Wang, J.; et al. Organotypic Hippocampal Slices as Models for Stroke and Traumatic Brain Injury. *Mol. Neurobiol*. **2016**, *53*, 4226–4237.
6. Rimann, M.; Graf-Hausner, U. Synthetic 3D Multicellular Systems for Drug Development. *Curr. Opin. Biotechnol*. **2012**, *23*, 803–809.
7. Ranga, A.; Gjorevski, N.; Lutolf, M. P.; et al. Drug Discovery through Stem Cell–Based Organoid Models. *Adv. Drug Deliv. Rev*. **2014**, *69–70*, 19–28.
8. Peng, W.; Datta, P.; Ayan, B.; et al. 3D Bioprinting for Drug Discovery and Development in Pharmaceutics. *Acta Biomater*. **2017**, *57*, 26–46.
9. Holmes, A. M.; Charlton, A.; Derby, B.; et al. Rising to the Challenge: Applying Biofabrication Approaches for Better Drug and Chemical Product Development. *Biofabrication* **2017**, *9*, 033001.
10. Dutta, D.; Heo, I.; Clevers, H.; et al. Disease Modeling in Stem Cell–Derived 3D Organoid Systems. *Trends Mol. Med*. **2017**, *23*, 393–410.
11. Huch, M.; Knoblich, J. A.; Lutolf, M. P.; et al. The Hope and the Hype of Organoid Research. *Development* **2017**, *144*, 938–941.
12. Elliott, N. T.; Yuan, F. A Review of Three-Dimensional in Vitro Tissue Models for Drug Discovery and Transport Studies. *J. Pharm. Sci*. **2011**, *100*, 59–74.
13. Fennema, E.; Rivron, N.; Rouwkema, J.; et al. Spheroid Culture as a Tool for Creating 3D Complex Tissues. *Trends Biotechnol*. **2013**, *31*, 108–115.
14. Kelm, J. M.; Fussenegger, M. Microscale Tissue Engineering Using Gravity-Enforced Cell Assembly. *Trends Biotechnol*. **2004**, *22*, 195–202.
15. Poulet, C.; Wettwer, E.; Christ, T.; et al. Skeletal Muscle Stem Cells Propagated as Myospheres Display Electrophysiological Properties Modulated by Culture Conditions. *J. Mol. Cell. Cardiol*. **2011**, *50*, 357–366.
16. Wei, Y.; Li, Y.; Chen, C.; et al. Human Skeletal Muscle-Derived Stem Cells Retain Stem Cell Properties after Expansion in Myosphere Culture. *Exp. Cell Res*. **2011**, *317*, 1016–1027.
17. Westerman, K. A.; Penvose, A.; Yang, Z.; et al. Adult Muscle 'Stem' Cells Can Be Sustained in Culture as Free-Floating Myospheres. *Exp. Cell Res*. **2010**, *316*, 1966–1976.
18. Huang, Y. C.; Dennis, R. G.; Larkin, L.; et al. Rapid Formation of Functional Muscle In Vitro Using Fibrin Gels. *J. Appl. Physiol (1985)*. **2005**, *98*, 706–713.
19. Kang, H. W.; Lee, S. J.; Ko, I. K.; et al. A 3D Bioprinting System to Produce Human-Scale Tissue Constructs with Structural Integrity. *Nat. Biotechnol*. **2016**, *34*, 312–319.
20. Murphy, S. V.; Atala, A. 3D Bioprinting of Tissues and Organs. *Nat. Biotechnol*. **2014**, *32*, 773–785.
21. Sears, N. A.; Seshadri, D. R.; Dhavalikar, P. S.; et al. A Review of Three-Dimensional Printing in Tissue Engineering. *Tissue Eng. Part B Rev*. **2016**, *22*, 298–310.
22. Huang, J.; Li, G.; Wang, W.; et al. 3D Printing Guiding Stent Graft Fenestration: A Novel Technique for Fenestration in Endovascular Aneurysm Repair. *Vascular* **2017**, *25*, 442–446.
23. Leberfinger, A. N.; Ravnic, D. J.; Dhawan, A.; et al. Concise Review: Bioprinting of Stem Cells for Transplantable Tissue Fabrication. *Stem Cells Transl. Med*. **2017**, *6*, 1940–1948.
24. Park, J. Y.; Gao, G.; Jang, J.; et al. 3D Printed Structures for Delivery of Biomolecules and Cells: Tissue Repair and Regeneration. *J. Mat. Chem. B* **2016**, *4*, 7521–7539.
25. Loessner, D.; Meinert, C.; Kaemmerer, E.; et al. Functionalization, Preparation and Use of Cell-Laden Gelatin Methacryloyl-Based Hydrogels as Modular Tissue Culture Platforms. *Nat. Protoc*. **2016**, *11*, 727–746.
26. Blaeser, A.; Duarte Campos, D. F.; Puster, U.; et al. Controlling Shear Stress in 3D Bioprinting Is a Key Factor to Balance Printing Resolution and Stem Cell Integrity. *Adv. Healthc. Mater*. **2016**, *5*, 326–333.
27. Zhang, Y. S.; Khademhosseini, A. Advances in Engineering Hydrogels. *Science* **2017**, *356*, eaaf3627.
28. Gilbert, P. M.; Havenstrite, K. L.; Magnusson, K. E.; et al. Substrate Elasticity Regulates Skeletal Muscle Stem Cell Self-Renewal in Culture. *Science* **2010**, *329*, 1078–1081.
29. Rimann, M.; Angres, B.; Patocchi-Tenzer, I.; et al. Automation of 3D Cell Culture Using Chemically Defined Hydrogels. *J. Lab. Autom*. **2014**, *19*, 191–197.
30. Rimann, M.; Bono, E.; Annaheim, H.; et al. Standardized 3D Bioprinting of Soft Tissue Models with Human Primary Cells. *J. Lab. Autom*. **2016**, *21*, 496–509.
31. Tabebordbar, M.; Wang, E. T.; Wagers, A. J.; et al. Skeletal Muscle Degenerative Diseases and Strategies for Therapeutic Muscle Repair. *Annu. Rev. Pathol*. **2013**, *8*, 441–475.
32. Romanick, M.; Thompson, L. V.; Brown-Borg, H. M.; et al. Murine Models of Atrophy, Cachexia, and Sarcopenia in Skeletal Muscle. *Biochim. Biophys. Acta* **2013**, *1832*, 1410–1420.
33. Ng, R.; Banks, G. B.; Hall, J. K.; et al. Animal Models of Muscular Dystrophy. *Prog. Mol. Biol. Transl. Sci*. **2012**, *105*, 83–111.
34. Warden, S. J. Animal Models for the Study of Tendinopathy. *Br. J. Sports Med*. **2007**, *41*, 232–240.
35. Jespersen, B.; Tykocki, N. R.; Watts, S. W.; et al. Measurement of Smooth Muscle Function in the Isolated Tissue Bath—Applications to Pharmacology Research. *J. Vis. Exp*. **2015**, *95*, 52324.
36. Sakamoto, K.; McCarthy, A.; Smith, D.; et al. Deficiency of Lkb1 in Skeletal Muscle Prevents Ampk Activation and

Glucose Uptake During Contraction. *EMBO J*. **2005**, *24*, 1810–1820.
37. Ajay, M.; Gilani, A. U.; Mustafa, M. R.; et al. Effects of Flavonoids on Vascular Smooth Muscle of the Isolated Rat Thoracic Aorta. *Life Sci*. **2003**, *74*, 603–612.
38. Ginsborg, B. L.; Warriner, J. The Isolated Chick Biventer Cervicis Nerve-Muscle Preparation. *Br. J. Pharmacol. Chemother*. **1960**, *15*, 410–411.
39. Dennis, R. G.; Kosnik, P. E., II; et al. Excitability and Isometric Contractile Properties of Mammalian Skeletal Muscle Constructs Engineered In Vitro. *In Vitro Cell Dev. Biol. Anim*. **2000**, *36*, 327–335.
40. Powell, C. A.; Smiley, B. L.; Mills, J.; et al. Mechanical Stimulation Improves Tissue-Engineered Human Skeletal Muscle. *Am. J. Physiol. Cell Physiol*. **2002**, *283*, C1557–C1565.
41. Vandenburgh, H.; Shansky, J.; Benesch-Lee, F.; et al. Drug-Screening Platform Based on the Contractility of Tissue-Engineered Muscle. *Muscle Nerve* **2008**, *37*, 438–447.
42. Paxton, J. Z.; Grover, L. M.; Baar, K.; et al. Engineering an In Vitro Model of a Functional Ligament from Bone to Bone. *Tissue Eng. Part A* **2010**, *16*, 3515–3525.
43. Juhas, M.; Engelmayr, G. C., Jr.; Fontanella, A. N.; et al. Biomimetic Engineered Muscle with Capacity for Vascular Integration and Functional Maturation in Vivo. *Proc. Natl. Acad. Sci. U. S. A*. **2014**, *111*, 5508–5513.
44. Madden, L.; Juhas, M.; Kraus, W. E.; et al. Bioengineered Human Myobundles Mimic Clinical Responses of Skeletal Muscle to Drugs. *Elife* **2015**, *4*, e04885.
45. Soofi, S. S.; Last, J. A.; Liliensiek, S. J.; et al. The Elastic Modulus of Matrigel as Determined by Atomic Force Microscopy. *J. Struct. Biol*. **2009**, *167*, 216–219.
46. Noori, A.; Ashrafi, S. J.; Vaez-Ghaemi, R.; et al. A Review of Fibrin and Fibrin Composites for Bone Tissue Engineering. *Int. J. Nanomed*. **2017**, *12*, 4937–4961.
47. Fairbanks, B. D.; Schwartz, M. P.; Bowman, C. N.; et al. Photoinitiated Polymerization of Peg-Diacrylate with Lithium Phenyl-2,4,6-Trimethylbenzoylphosphinate: Polymerization Rate and Cytocompatibility. *Biomaterials* **2009**, *30*, 6702–6707.
48. Agrawal, G.; Aung, A.; Varghese, S.; et al. Skeletal Muscle-on-a-Chip: An In Vitro Model to Evaluate Tissue Formation and Injury. *Lab Chip* **2017**, *17*, 3447–3461.
49. Vandenburgh, H. High-Content Drug Screening with Engineered Musculoskeletal Tissues. *Tissue Eng. Part B Rev*. **2010**, *16*, 55–64.
50. Annac, A. Invivosciences and Myomics Announce Partnership. 2012 [cited February 15, 2018]. Available from: http://invivosciences.com/invivosciences-and-myomics-announce-partnership/.
51. Capote, J.; Bolanos, P.; Schuhmeier, R. P.; et al. Calcium Transients in Developing Mouse Skeletal Muscle Fibres. *J. Physiol*. **2005**, *564*(Pt 2), 451–464.
52. Olsson, K.; Cheng, A. J.; Alam, S.; et al. Intracellular Ca(2+)-Handling Differs Markedly between Intact Human Muscle Fibers and Myotubes. *Skelet. Muscle* **2015**, *5*, 26.